Solar-Terrestrial Physics. 2023. Vol. 9. Iss. 2. P. 3–8. DOI: 10.12737/stp-92202301. © 2023
A.S. Kirichenko, I.P. Loboda, A.A. Reva, A.S. Ulyanov, S.A. Bogachev. Published by INFRA-M Academic Publishing House

UDC 523.98
DOI: 10.12737/stp-92202301

Received March 03, 2023
Accepted April 18, 2023

LATITUDINAL DISTRIBUTION OF SOLAR MICROFLARES AND HIGH-TEMPERATURE PLASMA AT SOLAR MINIMUM

A.S. Kirichenko
Space Research Institute RAS,
Moscow, Russia, a.s.kiri4enko@gmail.com

I.P. Loboda
Space Research Institute RAS,
Moscow, Russia, i.p.loboda@gmail.com

A.A. Reva
Space Research Institute RAS,
Moscow, Russia, reva.antoine@gmail.com

A.S. Ulyanov
Space Research Institute RAS,
Moscow, Russia, ikiru@inbox.ru

S.A. Bogachev
Space Research Institute RAS,
Moscow, Russia, bogachev.sergey@gmail.com

Abstract. The paper analyzes the latitudinal distribution of high-temperature plasma (T>4 MK) and microflares on the solar disk during low solar activity in 2009. The distribution of A0.1–A1.0 microflares contains belts typical of ordinary flares of B class and higher. In total, we have registered 526 flares, most of which, about 96 %, occurred at high latitudes. About 4 % of microflares were found near the solar equator. We believe that they were formed by the residual magnetic field of previous solar cycle 23. Ordinary flares were almost not observed near the equator during this period. The number of microflares in the southern hemisphere was slightly higher than in the northern one. This differs from the distribution of ordinary flares for which the northern hemisphere was previously reported to be dominant.

Keywords: microflares, solar cycle, plasma heating.

INTRODUCTION

Spatial distribution of active regions and X-ray flares (excluding microflares (energy 10^{27}–10^{30} erg) and nanoflares (energy 10^{24}–10^{27} erg)) over the Sun is very nonuniform. Flares and sunspot groups are generally formed in the so-called activity belts whose location depends on solar cycle phase [Rao, 1974]. The belts arise at the beginning of a cycle at high latitudes, then slowly shift toward the equator, which, when their latitude dependence is plotted, makes up the well-known butterfly diagram [Knoska, Krivsky, 1978].

There are many works that examine the spatial distribution of flares, which agree that the reason for the peculiarities of their localization is the nonuniform structure of the solar magnetic field. Howard [1974], for one, has analyzed the period from 1967 to 1973 and has shown that 95 % of the magnetic flux in both solar hemispheres is in the latitude range from 0° to 40°. The absolute majority of solar flares are recorded within this latitude range, regardless of solar cycle phase.

A number of papers study the asymmetry of activity in the southern and northern hemispheres of the Sun. For example, Bell [1962] showed the presence of long-term asymmetry for solar cycles with numbers from 8 to 18. It was demonstrated that during cycles 8, 9, and from 14 to 18, activity prevailed in the northern hemisphere — the corresponding percentage of sunspots varied from 50 to 60 %. Verma et al. [1987] have indicated that during solar cycles 19 and 20 most flares occurred in the northern hemisphere. Verma and Joshi [1987] have demonstrated that during solar cycle 21 activity prevailed in the southern hemisphere. Yadav and Badruddin [1980] have analyzed the latitudinal distribution of optical flares in the southern and northern hemispheres from 1957 to 1978 and have revealed that 64 % of all flares occurred in the northern hemisphere; and only 36 %, in the southern hemisphere. At the same time, from 1957 to 1970 there were a larger number of optical flares in the northern hemisphere; and from 1970 to 1978, in the southern hemisphere, with the spatial distribution of flares changing not between two cycles, but directly during the cycle. Garcia [1990], analyzing solar flares of the X-ray class M1 and higher, has revealed that in solar cycles 20 and 21 the northern hemisphere was first more active, and then the activity shifted to the southern hemisphere. In cycle 22, according to [Li et al., 1998], the southern hemisphere was more active. Joshi et al. [2006] by examining the distribution of chromospheric flares in the Hα line have shown that at the beginning of cycle 23 most flares were recorded in the northern hemisphere and, after passing the maximum, in the southern hemisphere. A large number of flares of class C and higher from 1976 to 2008 have been analyzed in [Pandey et al., 2015]. The authors confirmed the asymmetry of solar activity during the period between cycles 21 and 23. The results of these studies are in good agreement and indicate that the asymmetry of X-ray flares from cycle 21 to cycle 23 varied from –0.8 to 0.3. The data obtained is also confirmed by the analysis of synoptic charts carried out in [Yazev et al., 2021]. Joshi et al. [2010] have analyzed solar activity for the period from 1976 to 2007 and have revealed that the maximum asymmetry in the spatial location of flares and sunspots is observed at solar minimum.

The question about the spatial distribution of low-energy flares is still much less understood (see, e.g., the review [Bogachev et al., 2020]). A large number of flares of low X-ray classes from A to C (more than 25 000 events) have been studied in [Christe et al., 2008], using data from the RHESSI X-ray telescope and the GOES X-ray monitor. The authors have drawn a conclusion that there are belts in the spatial distribution of the events considered, as well as in the distribution of ordinary flares of C class and higher.

Reva et al. [2012] have examined 169 events identified as hot X-ray points (HXPs). HXPs are short-lived (5–100 min) high-temperature (5–50 MK) objects, which distinguishes them, for instance, from X-ray bright points whose lifetime may be 8–40 hrs, and the temperature does not exceed several million degrees. The study was based on X-ray solar images captured by the CORONAS-F spacecraft (see [Zhitnik et al., 2003]). Reva et al. [2012] have indicated that most HXPs are located in activity belts in contrast to X-ray bright points having a uniform spatial distribution [Golub et al., 1974]. A small number of HXPs have been detected near the equator.

Borovik and Zhdanov in [2018, 2019, 2020] have studied the flare events that can be considered as extremely powerful microflares, using data in the Hα line. It was found that during four solar cycles after cycle 21 there was a significant decrease in the number of flare events recorded in the optical range. Unfortunately, statistics on the spatial location of flares on the solar disk is not given in these works.

Kirichenko and Bogachev (see, e.g., [Kirichenko, Bogachev, 2013; Kirichenko, Bogachev, 2017a, b] have developed methods for finding and determining coordinates of weak flares (microflares) of X-ray class below A1.0. Using these methods, they discovered a correlation between class of microflares and magnetic field characteristics, but did not pay attention to the spatial distribution of microflares.

In this paper, we modify the methods from [Kirichenko, Bogachev, 2013; Kirichenko, Bogachev, 2017a, b] and apply them to the spatial distribution of microflares of X-ray class A0.1 and higher and to the spatial distribution of hot plasma formed in the microflares. We want to figure out whether the activity belts remain in this range, or flares are distributed more evenly. We suppose that low-energy flares should have a uniform distribution. Such events can develop in compact regions with a weak magnetic field, the conditions for the existence of which can be provided at any latitudes. However, the question as to where the transition from belts to uniform distribution takes place (in microflares, nanoflares or picoflares (energy 10^{21}–10^{24} erg)) and whether it occurs at all has not yet been unequivocally resolved. For the study, we have chosen the period of low solar activity in 2009, which we considered favorable for investigating low-energy flares.

The structure of the paper is as follows. In the next section, we briefly describe the data used and processing methods. Section 2 presents the results. In section 3, we discuss the results and draw scientific conclusions.

1. DATA AND METHODS

For the study, we have mainly used data from CORONAS-Photon spacecraft instruments operating in 2009: 1) solar telescope FET; 2) imaging spectroheliometer MISH [Kuzin et al., 2009; Kuzin et al., 2011]; 3) X-ray spectrophotometer SphinX [Gburek, 2013].

Coordinates of microflares were determined from MISH data; the imaging spectroheliometer detects micro-events by X-ray emission from the plasma they heat. This instrument is monochromatic, i.e. it records emission in a very narrow wavelength range with only one strong spectral line — the MgXII doublet (8.419 and 8.425 Å wavelengths; see description of the instrument in [Reva et al., 2021]). Since MISH has a very high threshold of temperature sensitivity (from 3–4 million kelvin), it can provide data on hot microflares against the background of a colder plasma of the quiet corona and active regions. An image captured by MISH during the period of interest is displayed on the right panel of Figure 1. The left panel shows a close-in-time solar image in a colder spectral region (171 Å; T~0.6 million kelvin), obtained by the solar telescope FET.

To determine the X-ray class of microflares, we have used data from the SphinX spectrophotometer. The instrument recorded soft X-ray spectra in the range 1–15 keV, as well as in the wavelength range 1–8 Å, employed for X-ray classification of flares. Information on SphinX calibration, time profile processing features, and the method for determining the X-ray class of flares can be found in [Gryciuk et al., 2017]. SphinX had a sensitivity in 1–8 Å sufficient to detect flares of the X-ray class A0.1 and higher. Also noteworthy is the low level of background X-ray emission from the Sun during the period under study, which was predominantly below the sensitivity threshold of GOES monitors, which corresponds to the A1 class. This fact is crucially important for the correct assessment of flare class when using the instrument that records the emission flux from the entire solar disk.

2. RESULTS

2.1. Spatial distribution of high-temperature radiation sources

The spatial distribution of all high-temperature radiation sources found in MISH images (11109 events) is illustrated in Figure 2. The upper panel illustrates the distribution of radiation sources over the solar disk. The solar minimum between cycles 23 and 24 occurred approximately in December 2008. For this reason, in 2009 on the Sun there were simultaneously the activity centers located near the equator and associated with the end of solar cycle 23, as well as the activity centers of new cycle 24, located at high latitudes. High-latitude radiation sources in the northern and southern hemispheres are shown respectively in blue and red colors on the top panel of Figure 2. Radiation sources near the equator are shown in white.

In general, the distribution of high-temperature plasma revealed good agreement with the expected structure of activity belts at solar minimum.

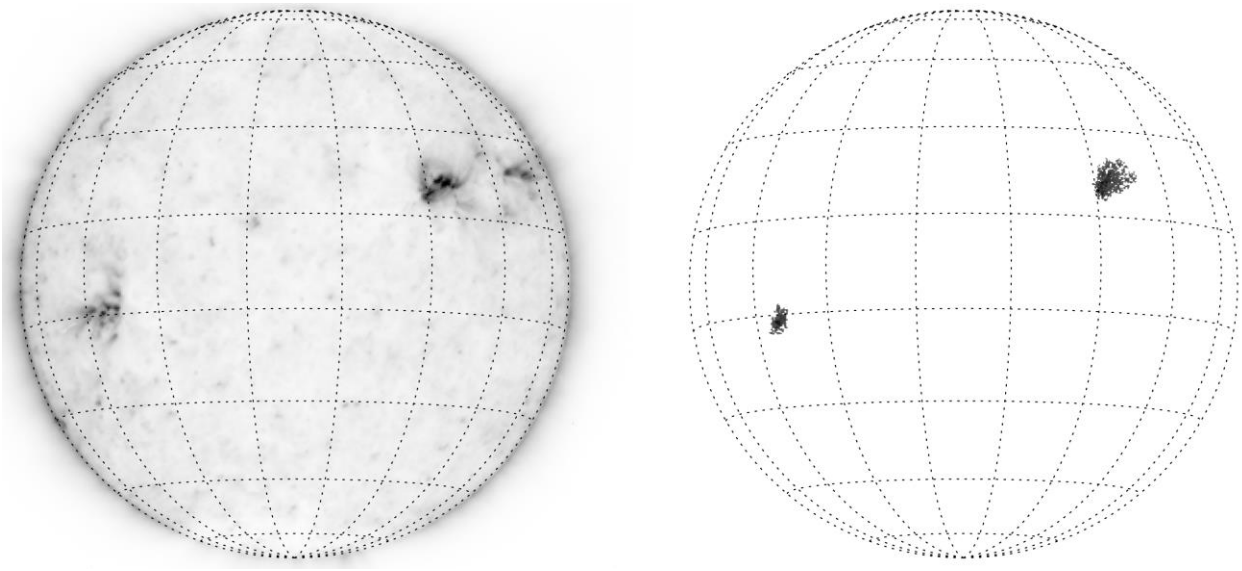

Figure 1. Examples of solar images we use in the work: a solar image captured by the FET telescope in the 171 Å line (left); a close-in-time solar image obtained by the MISH spectroheliometer in the 8.42 Å line (right)

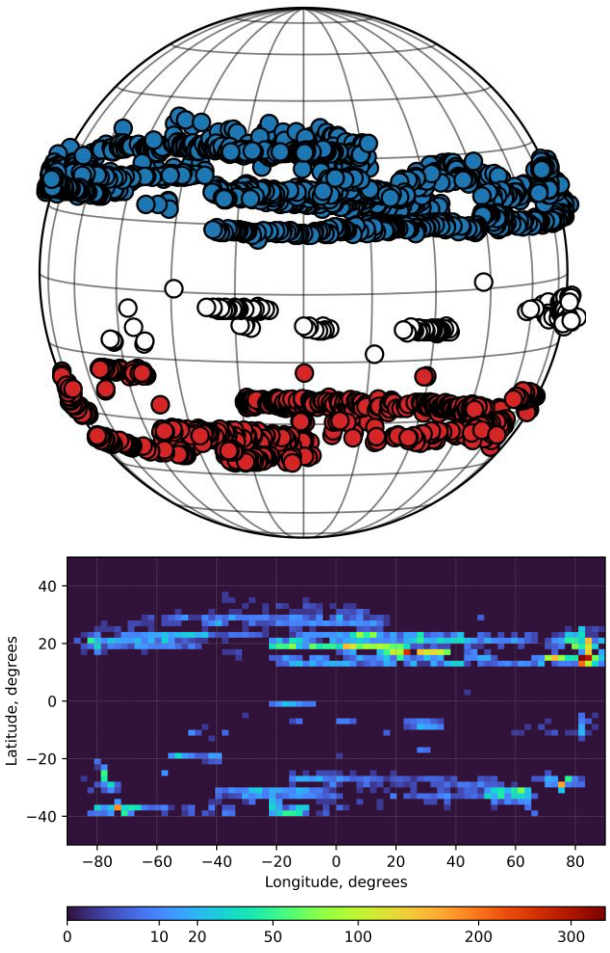

Figure 2. Spatial distribution of high-temperature (T>4 MK) radiation sources over the solar disk in 2009 (solar minimum) derived from CORONAS-Photon spacecraft data

The bottom panel of Figure 2 represents the same result as a chart: distribution of radiation sources along latitude and longitude. The color scale indicates the number of sources detected in the corresponding regions on the solar disk. As on the top panel, the distribution structure in the form of three belts is clearly seen: two belts at high latitudes and one group near the equator. The longitude of 0° corresponds to the central meridian of the Sun when observed from Earth. The longitudes of –90° and +90° correspond to the eastern and western limbs of the solar disk. We did not determine the absolute (Carrington) longitude of the radiation sources because we did not aim at examining the longitude distribution.

2.2. Spatial distribution of microflares

Spatial distribution of microflares, i.e. the radiation sources for which the emission profile was reliably measured and the X-ray class (526 events) was defined is shown in Figure 3.

As for high-temperature radiation sources (Figure 2), three groups are seen in Figure 3: two belts at high latitudes (in the northern hemisphere (blue), in the southern hemisphere (red)) and one group near the equator (white).

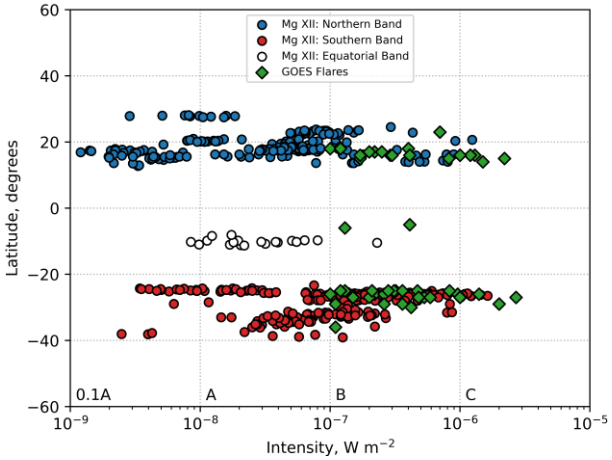

Figure 3. Latitude distribution of solar microflares in 2009 (solar minimum) derived from CORONAS-Photon and GOES SC data

The green color indicates flares from the GOES catalog, whose coordinates were not found in MISH data, but were taken from the NOAA catalog.

Along the X-axis is an X-ray class of a flare (A, B, C) and the emission flux intensity in the range 1–8 Å (W m^{-2}). The flares found from GOES data have approximately B class and higher. The flares found from MISH and SphinX data have a class from A0.1 and higher.

3. DISCUSSION

The solar minimum is characterized by favorable conditions for observing low-energy flares. In 2009, the CORONAS-Photon spacecraft operated in Earth's orbit, providing a significant amount of data on solar activity during this period. In this study, we have used the data to analyze the spatial distribution of low-energy flares and high-temperature radiation sources.

From the results of data processing we have found a significant number of high-temperature radiation sources (11109) for which it was possible to determine their position on the solar disk. Unfortunately, only for a small percentage of these sources we could reliably measure the emission profile, as well as estimate the X-ray class. This is primarily due to the difficulty in identifying weak bursts against a background of noise. In particular, the X-ray detectors operating at that time on board the GOES spacecraft (SC) reliably detected only flares of B class and higher. Moreover, part of the data from the SphinX instrument we use in our work was lost because the CORONAS-Photon spacecraft was in radiation belts. In total, we have determined coordinates for 475 microflares of the X-ray class A0.1 and higher from MISH and SphinX data; and for another 51 flares of B class and higher, from GOES SC data.

The latitude distributions of flares and high-temperature plasma (see Figures 2 and 3) turned out match the expected distribution, which follows from Spoerer's law. Figure 4 presents a butterfly diagram for the period from 1996 to 2020. According to the data, three groups of flares should have been observed in 2009: two at high latitudes in the northern and southern hemispheres and one near the equator. Both distributions we have obtained (both for high-temperature plasma and for microflares) roughly fit this pattern.

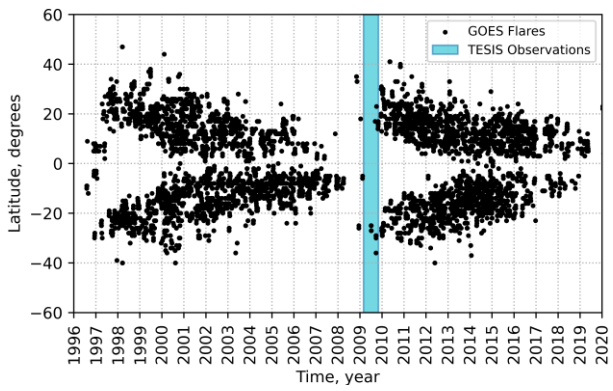

Figure 4. Latitude distribution of solar flares of B class and higher during solar cycles 23 and 24 as derived from GOES and NOAA catalogs. The period we deal with (TESIS observations) is shown

It was difficult to draw reliable conclusions about the distribution of flares in the period of interest only from GOES SC data since we found only 51 events of B class and higher in the corresponding catalog. The conclusions drawn in this work have been made only due to the use of MISH and SphinX data on flares of A0.1 class and higher.

Note also that it is almost impossible to separate the high-latitude flare belts from the near-equator region, using only GOES data. For example, Abdel-Sattar et al. [2018] did not manage to identify a distribution region near the equator: this group appeared to be mixed with the wings of the southern and northern belts. In our case, of all the flares recorded by GOES only two events have been reliably attributed to the equatorial region. All other flares of this group have been found from SphinX and MISH data. The events of the equatorial group accounted for 4.2 % of the total number of flares.

The distribution of flares in the belts is not symmetric and cannot be approximated by a simple function, such as the Gaussian distribution. Figure 5 exhibits the actual latitude distribution of high-temperature radiation sources (top panel) and microflares (bottom panel). The red curve in Figure 5 is the result of approximation of the distribution by the sum of the Gaussian function and the second-degree polynomial. We can see that the internal and external parts of the distribution in both the northern and southern hemispheres have different variance, but we have not studied this issue in more detail.

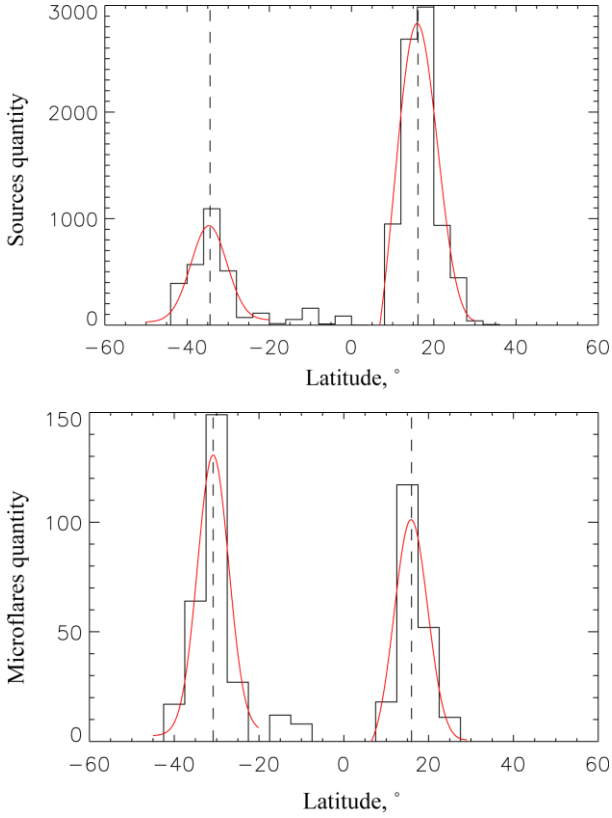

Figure 5. Actual latitude distribution of high-temperature radiation sources (top panel) and microflares (bottom panel). The red curve is the approximation result

Some statistical information on distributions of flares and high-temperature plasma is given in Table 1. The information is given only for high-latitude belts: northern and southern. The equatorial distribution is not presented because, due to the small number of events, statistical conclusions about it are unreliable.

The distributions in Figure 5 show an asymmetry in the number of events in the northern and southern hemispheres. To quantify it, we use the formula:

$$A = \frac{N - S}{N + S},$$

where N is the number of events in the northern hemisphere; and S, in the southern hemisphere. $A>0$ corresponds to the case when the largest number of events has been recorded in the northern hemisphere; and $A<0$, in the southern hemisphere. The results are presented in Table 2.

The results obtained are somewhat contradictory as they lead to different conclusions for high-temperature plasma and microflares. In the former case, the northern hemisphere was significantly dominated by the number of events; and in the latter case, the southern hemisphere was slightly dominated. This difference can be explained by the possibility of hot plasma formation in the corona not only in flares, but also due to slow energy release in active regions (see, e.g., [Grechnev et al., 2006; Urnov et al., 2007]). Note that in [Abdel-Sattar et al., 2018] for a longer period from 2008 to 2012, which included 2009 we study, an asymmetry was found with a predominance of activity for flares in the northern hemisphere (5861 events in the southern hemisphere versus 10407).

Note that in Figure 3 there is an increase in the width of the belt in the region of weak microflares (X-ray class below A1.0) compared to flares of B class and higher. In other words, there are signs of an increase in the latitude range within which flare events are recorded as their power decreases. We find this interesting because we believe that when approaching the lowest-energy flares (nanoflares and, possibly, picoflares) the latitude distribution should become more uniform (see, e.g., new results on nanoflares in [Zavershinsky et al., 2022; Bogachev, Erkhova, 2023]). It appears likely that we see signs of just such a transition in Figure 3. However, the accuracy of the data we have obtained is not yet sufficient for a reliable conclusion in this regard due to the small statistics, as well as the lack of data for the events whose class is lower than A0.1.

Table 1

Characteristics of latitude distributions of high-temperature radiation sources and microflares

Sample	Group	Mean latitude, deg	Latitude range, deg
High-temperature plasma	Northern	18.6°±3.9°	from 12° to 36.4°
	Southern	–32.4°±4.4°	from –39.7° to –17.2°
Microflares	Northern	18.5°±3.4°	from 12.8° to 28.1°
	Southern	–28.3°±3.7°	from –39.1° to –23.3°

Table 2

Asymmetry of distributions in the northern and southern hemispheres during the period under study

Sample	Asymmetry
High-temperature plasma	0.49
Microflares	–0.13

The work was financially supported by the Russian Science Foundation (Grant No. 21-72-10157).

REFERENCES

Abdel-Sattar W., Mawad R., Moussas X. Study of solar flares' latitudinal distribution during the solar period 2002–2017: GOES and RHESSI data comparison. *Adv. Space Res*. 2018, vol. 62, no. 9, pp. 2701–2707. DOI: 10.1016/j.asr.2018.07.024.

Bell B. A long-term north-south asymmetry in the location of solar sources of great geomagnetic storms. *Smithsonian Contr. Astrophys.* 1962, vol. 5, p. 203.

Bogachev S.A., Erkhova N.F. Measurement of energy distribution for low power nanoflares. *Solar-Terrestrial Physics.* 2023, vol. 9, iss. 1, pp. 3–8. DOI: 10.12737/stp-91202301.

Bogachev S.A., Ulyanov A.S., Kirichenko A.S., Loboda I.P., Reva A.A. Microflares and nanoflares in the solar corona. *Physics-Uspekhi*. 2020, vol. 63, iss. 8, pp. 783–800. DOI: 10.3367/UFNe.2019.06.038769.

Borovik A.V., Zhdanov A.A. Statistical studies of duration of low-power solar flares. *Solar-Terrestrial Physics*. 2018, vol. 4, iss. 2, pp. 8–16. DOI: 10.12737/stp-42201803.

Borovik A.V., Zhdanov A.A. Processes of energy release in low-power solar flares. *Solar-Terrestrial Physics*. 2019, vol. 5, iss. 4, pp. 3–9. DOI: 10.12737/stp-54201901.

Borovik A.V., Zhdanov A.A. Low-power solar flares of optical and X-ray wavelengths for solar cycles 21–24. *Solar-Terrestrial Physics*. 2020, vol. 6, iss. 3, pp. 16–22. DOI: 10.12737/stp-63202002.

Christe S., Hannah I.G., Krucker S., McTiernan J., Lin R.P. RHESSI microflare statistics. I. Flare-finding and frequency distributions. *Astrophys. J.* 2008, vol. 677, no. 2, p. 1385. DOI: 10.1086/529011.

Garcia H.A. Evidence for solar-cycle evolution of north-south flare asymmetry during solar cycle 20 and 21. *Solar Phys*. 1990, vol. 127, p. 185. DOI: 10.1007/BF00158522.

Gburek S., Sylwester J., Kowalinski M., Bakala J., Kordylewski Z., Podgorski P., Plocieniak S., et al. SphinX: The Solar Photometer in X-rays. *Solar Phys.* 2013, vol. 283, pp. 631–649. DOI: 10.1007/s11207-012-0201-8.

Golub L., Krieger A.S., Silk J.K., Timothy A.F., Vaiana G.S. Solar X-ray bright points. *Astrophys. J. Lett.* 1974, vol. 189, p. L93. DOI: 10.1086/181472.

Grechnev V.V., Kuzin S.V., Urnov A.M., Zhitnik I.A, Uralov A.M., Bogachev S.A., Livshits M.A., et al. Long-lived hot coronal

structures observed with CORONAS-F/SPIRIT in the Mg XII line. *Solar System Res*. 2006, vol. 40, pp. 286–293. DOI: 10.1134/S0038094606040046.

Gryciuk M., Siarkowski M., Sylwester J., Gburek S., Podgorski P., Kepa A., Sylwester B., Mrozek T. Flare characteristics from X-ray light curves. *Solar Phys.* 2017, vol. 292, 77. DOI: 10.1007/s11207-017-1101-8.

Howard R. Studies of Solar Magnetic Fields. II: The Magnetic Fluxes. *Solar Phys*. 1974, vol. 38. pp. 59–67. DOI: 10.1007/BF00161823.

Joshi N.C., Bankoti N.S., Pande S., Pande B., Uddin W., Pandey K. Statistical analysis of soft X-ray solar flares during solar cycles 21, 22 and 23. *New Astron.* 2010, vol. 15, pp. 538–546. DOI: 10.1016/j.newast.2010.01.002.

Joshi B., Pant P., Manoharan P.K. North-South distribution of solar flares during cycle 23. *J. Astrophys. Astron*. 2006, vol. 27, p. 151–157. DOI: 10.1007/BF02702517.

Kirichenko A.S., Bogachev S.A. Long-duration plasma heating in solar microflares of X-ray class A1.0 and lower. *Astron. Lett.* 2013, vol. 39, pp. 797–807. DOI: 10.1134/S1063773713110042.

Kirichenko A.S., Bogachev S.A. Plasma heating in solar microflares: Statistics and analysis. *Astrophys. J.* 2017a, vol. 840, no. 1, pp. 45–52. DOI: 10.3847/1538-4357/aa6c2b.

Kirichenko A.S., Bogachev S.A. The relation between magnetic fields and X-ray emission for solar microflares and active regions. *Solar Phys*. 2017b, vol. 292, pp.120–134. DOI: 10.1007/s11207-017-1146-8.

Knoska S., Krivsky L. Time-latitude occurence of flares in solar cycle No 20 (1965–1976). *Bull. Astron. Inst. Czechoslov*. 1978, vol. 29, p. 352.

Kuzin S.V., Bogachev S.A., Zhitnik I.A., Pertsov A.A., Ignatiev A.P., Mitrofanov A.M., Slemzin V.A., et al. TESIS experiment on EUV imaging spectroscopy of the Sun. *Adv. Space Res.* 2009, vol. 43, no. 6, pp. 1001–1006. DOI: 10.1016/ j.asr.2008.10.021.

Kuzin S.V., Zhitnik I.A., Shestov S.V., Bogachev S.A., Bugaenko O.I., Ignat'ev A.P., Pertsov A.A., Ulyanov A.S., et al. The TESIS experiment on the CORONAS-PHOTON spacecraft. *Solar System Res*. 2011, vol. 45, pp. 162–173. DOI: 10.1134/S0038094611020110.

Li K.J., Schmieder B., Li Q.Sh. Statistical analysis of the X-ray flares (M>=1) during the maximum period of solar cycle 22. *Astron. Astrophys. Suppl. Ser*. 1998, vol. 131, pp. 99–104. DOI: 10.1051/aas:1998254.

Pandey K.K., Yellaiah G., Hiremath K.M. Latitudinal distribution of soft X-ray flares and dispairty in butterfly diagram. *Astrophys. Space Sci*. 2015, vol. 356, pp. 215–224. DOI: 10.1007/s10509-014-2148-8.

Rao K.R. Latitudinal distributions of solar optical flares. *Proc. International Symposium on Solar-Terrestrial Physics. Sao Paulo, Brazil.* 1974, vol. 1, pp. 4–15.

Reva A., Shestov S., Bogachev S., Kuzin S. Investigation of Hot X-Ray Points (HXPs) using spectroheliograph Mg XII experiment data from CORONAS-F/SPIRIT. *Solar Phys.* 2012, vol. 276, pp. 97–112. DOI: 10.1007/s11207-011-9883-6.

Reva A.A., Kuzin S.V., Kirichenko A.S., Ulyanov A.S., Loboda I.P., Bogachev S.A. Monochromatic X-ray imagers of the Sun based on the Bragg crystal optics. *Front. Astron. Space Sci*. 2021, vol. 8. DOI: 10.3389/fspas.2021.645062.

Urnov A.M., Shestov S.V., Bogachev S.A., Goryaev F.F., Zhitnik I.A., Kuzin S.V. On the spatial and temporal characteristics and formation mechanisms of soft X-ray emission in the solar corona. *Astron. Lett.* 2007, vol. 33, pp. 396–410. DOI: 10.1134/S1063773707060059.

Verma V.K., Pande M.C., Wahab U. Energetic flare zones on the Sun. *Solar Phys.* 1987, vol. 112, pp. 341–346. DOI: 10.1007/BF00148788.

Verma V.K., Joshi G.C. On the periodicities of sunspots and solar strong hard X-ray bursts. *Solar Phys.* 1987, vol. 114, pp. 415–418. DOI: 10.1007/BF00167358.

Yadav R.S., Badruddin K.S. Solar latitudinal distribution of solar flares of different importances around the Sun. *Indian J. Radio Space Phys*. 1980, vol. 9, p. 155.

Yazev S.A., Ulianova M.M., Isaeva E.S. Complexes of activity on the Sun in solar cycle 21. *Solar-Terrestrial Physics.* 2021, vol. 7, iss. 4, pp. 3–9. DOI: 10.12737/stp-74202101.

Zavershinsky D.I., Bogachev S.A., Belov S.A., Ledentsov L.S. Method for searching nanoflares and their spatial distribution in the solar corona. *Astron. Lett*. 2022, vol. 48, no. 9, pp. 550–560. DOI: 10.1134/S1063773722090079.

Zhitnik I., Kuzin S., Afanas'ev A., Bugaenko O., Ignat'ev A., Krutov V., Mitrofanov A., Oparin S., Pertsov A., et al. XUV observations of solar corona in the SPIRIT experiment on board the CORONAS-F satellite. *Adv. Space Res.* 2003, vol. 32, pp. 473–477. DOI: 10.1016/S0273-1177(03)00351-X.

Original Russian version: Kirichenko A.S., Loboda I.P., Reva A.A., Ulyanov A.S., Bogachev S.A., published in Solnechno-zemnaya fizika. 2023. Vol. 9. Iss. 2. P. 5–11. DOI: 10.12737/szf-92202301.

How to cite this article

Kirichenko A.S., Loboda I.P., Reva A.A., Ulyanov A.S., Bogachev S.A. Latitudinal distribution of solar microflares and high-temperature plasma at solar minimum. *Solar-Terrestrial Physics.* 2023. Vol. 9. Iss. 2. P. 3–8. DOI: 10.12737/stp-92202301.